Received: 23 February 2023 | Revised: 27 July 2023 | Accepted: 22 August 2023

DOI: 10.1002/btpr.3388

BIOTECHNOLOGY PROGRESS

RESEARCH ARTICLE

Biocatalysts and Bioreactor Design

Development of a centrifugal bioreactor for rapid expansion of CD8 cytotoxic T cells for use in cancer immunotherapy

Kitana M. Kaiphanliam[1] | Brenden Fraser-Hevlin[1] | Eric S. Barrow[2] | William C. Davis[3] | Bernard J. Van Wie[1]

[1]Voiland School of Chemical Engineering and Bioengineering, Washington State University, Pullman, Washington, USA

[2]Voiland College of Engineering and Architecture Professional Shops, Washington State University, Pullman, Washington, USA

[3]Department of Veterinary Microbiology and Pathology, Washington State University, Pullman, Washington, USA

Correspondence
Bernard J. Van Wie, Voiland School of Chemical Engineering and Bioengineering (VSCEB), Washington State University (WSU), 1505 NE Stadium Way, Pullman, WA 99164-6515, USA.
Email: bvanwie@wsu.edu

Funding information
National Science Foundation, Grant/Award Number: 1645249; Washington Research Foundation; Washington State University (Commercialization Gap Fund 2021, Palouse Club Cougar Cage 2021)

Abstract

One of the current difficulties limiting the use of adoptive cell therapy (ACT) for cancer treatment is the lack of methods for rapidly expanding T cells. As described in the present report, we developed a centrifugal bioreactor (CBR) that may resolve this manufacturing bottleneck. The CBR operates in perfusion by balancing centrifugal forces with a continuous feed of fresh medium, preventing cells from leaving the expansion culture chamber while maintaining nutrients for growth. A bovine CD8 cytotoxic T lymphocyte (CTL) cell line specific for an autologous target cell infected with a protozoan parasite, *Theileria parva*, was used to determine the efficacy of the CBR for ACT purposes. Batch culture experiments were conducted to predict how CTLs respond to environmental changes associated with consumption of nutrients and production of toxic metabolites, such as ammonium and lactate. Data from these studies were used to develop a kinetic growth model, allowing us to predict CTL growth in the CBR and determine the optimal operating parameters. The model predicts the maximum cell density the CBR can sustain is 5.5×10^7 cells/mL in a single 11-mL conical chamber with oxygen being the limiting factor. Experimental results expanding CTLs in the CBR are in 95% agreement with the kinetic model. The prototype CBR described in this report can be used to develop a CBR for use in cancer immunotherapy.

KEYWORDS
biomanufacturing, bioprocessing, immunotherapy, mammalian cell kinetics, T cells

1 | INTRODUCTION

Cancer remains one of the leading causes of death in the United States and worldwide.[1,2] This is attributable in part to the difficulties in detecting cancers early before they begin to metastasize and in part the challenges in developing targeted therapies specific for the different forms of cancer. Most of the current therapies are non-targeted, where the strategy is to treat with radiation or different drugs in which the level of toxicity is greater for the malignant cell than toxicity for normal cells; however, negative side effects are prevalent. Some progress has been made in developing therapies using drugs designed to target gene mutations that occur in some types of malignancies as reviewed in Nature Communications.[3] The most promising form of therapy, still in the early stages of development though, is immunotherapy. Studies focused on explaining the basis for spontaneous resolution of some forms of cancer revealed resolution was associated with the development of an immune response that cleared the malignancy. Analysis at the cellular level demonstrated clearance was mediated by CD8 cytotoxic T lymphocytes (CTLs). Follow-up studies have demonstrated that CD8 CTLs could be isolated and used to clear some forms of cancer as reviewed recently by authors Farhood et al.[4]

Extensive investigations are now in progress to develop strategies to bring the potential of immunotherapy from the bench to the bedside: (1) modulate the host immune system to potentiate the capacity of CD8 CTLs to kill cancer cells, (2) develop methods to generate genetically modified CTLs that are able to kill cancer cells, and (3) develop a bioreactor for culture and rapid expansion of natural or genetically modified CTLs for use in immunotherapy.[5] The latter approach offers an opportunity to provide a continuous source of host-derived or genetically modified CTLs in case multiple infusions are needed. A review of current approaches to cell manufacturing has shown further research is needed to develop a bioreactor for the rapid expansion of CTLs. Current solutions include the G-Rex® by Wilson Wolf Manufacturing,[6] the Xuri™ W25 by Cytiva Life Sciences,[7] the CliniMACS Prodigy® by Miltenyi Biotec,[8] and the Cocoon® by Lonza.[9] The G-Rex® system expands T cells much like traditional static culture solutions but incorporates a gas-permeable membrane to promote gas exchange. The Xuri™, CliniMACS Prodigy®, and Cocoon® are all automated systems that operate in fed-batch or continuous modes each equipped with their own mechanism for gas exchange. Although the automation and mitigation of certain steps in the overall cell culturing process make these systems easier to use, none of the expansion systems developed thus far have resolved key manufacturing bottlenecks in continuous cell culture—prevention of cell product loss or washout while simultaneously removing inhibitory waste product.[10]

The approach we have taken to overcome this manufacturing bottleneck is development of a centrifugal bioreactor (CBR). The bioreactor design was inspired by COBE® instrumentation intended for on-site separation of blood by density gradient for continuous harvest and return of specific blood components.[11] An anti-twister mechanism was devised to maintain individual streams for separation. These design concepts were used to develop the CBR intended to maintain cells in suspension in a conical culture chamber by balancing high centrifugal forces with opposing drag and buoyant forces provided by a constant stream of medium introduced into the chamber toward the rotor disc center.[12] Early experiments were conducted by modifying a COBE® Spectra Apheresis machine and replacing the blood separation components with conical cell culture chambers.[13] Results from these studies demonstrated it is possible to expand and maintain cell cultures at high densities on the order of 10^8 cells/mL. The initial research provided the basic technical information needed to develop a prototype CBR for use in cancer immunotherapy.

In the present report, we describe engineering innovations used to construct and test a prototype CBR with a proof-of-concept CD8 CTL target cell system. Static culture experiments determine growth parameters for a kinetic model to optimize cell growth in the CBR, evaluating consumption of glucose and dissolved oxygen (DO) and production of inhibitory metabolites, lactate, and ammonium.[14] The overarching research question addressed is whether data support the hypothesis that the CBR technology is useful for biomanufacturing clinically relevant numbers of CTLs in the context of cancer immunotherapy.

2 | MATERIALS AND METHODS

2.1 | Construction of a benchtop CBR

The initial proof of concept studies demonstrating cells could be cultured in suspension in a conical CBR culture chamber were performed during 1986 through 1991.[12,15] The results demonstrated the potential of developing a CBR for use in immunological investigations. Recent studies reveal a major impediment in the adoption of cancer immunotherapy is limited manufacturing devices for rapid expansion of CD8 CTLs.[5] This provided an incentive to accelerate development of a CBR for research and cancer immunotherapy. We modified a COBE® Spectra Apheresis machine for proof-of-concept research purposes (Figure 1a). Although useful for ongoing studies, it was clear that a miniaturized, stand-alone CBR would need to be developed and made available for adoption by the research and clinical immunotherapy communities.

To allow the prototype to act as a stand-alone system, we designed a biosafety-cabinet-inspired encasement to house the CBR with additional cabinets to contain associated operating equipment and supplies. We integrated a compact, 3 stage, 0.3-micron HEPA filtration system (Koios HA1122-1) and user-controlled 8W T5 germicidal ultraviolet-C (UVC) light (McMaster-Carr 9188K12) to keep an aseptic environment. For the anti-twister mechanism, gears were arranged in varying directions and ratio to control the sample disk rotation speed while counter-rotating the connected tubes as outlined in a patent application currently in review and prior work.[16,17] Safety measures were integrated such as a fully guarded framework using 3 mm 6061 aluminum side panels along with double layer 6 mm polycarbonate and 6 mm acrylic panels for projectile and UV protection while maintaining a clear view of operation and a separate easy-to-identify external emergency stop switch. Access to the centrifuge bay is protected by an auto-stop limit switch to protect the user from exposure to rapidly rotating hardware, prohibiting operation unless the door is fully closed with the spring-loaded lock in position. To drive rotation, we used a Marathon XRI series 0.75 HP vector duty motor capable of 0–1800 RPM connected via a 6-band v-belt underneath the unit, paired with a programmable variable frequency drive (DURApulse GS20). The user interface incorporates complete digital control to adjust rotor speeds, motor ramp up and down speed, fluid flow rates, switches for power, lights, fans, and independent programmable temperature control for two housings. PTC ceramic air heaters and 12 V DC powered fans to maintain temperature at 37°C for cell cultures. Peristaltic pumps were calibrated in house with Flexelene™ tubing (U.S. Plastic Corp. 65063), which was the tubing chosen for all connecting lines as it is intended for bioprocesses, and pump speeds were individually set based on calibration results. DO was continuously monitored through flow cells with fiber optic sensors and complementary DOTS™ software as part of a beta-testing collaboration with Scientific Bioprocessing, Inc. (SBI). The process flow diagram for the system is shown in Figure 1b and indicates where individual units are housed within the different encasements. Not included in the flow diagram are the electronic units controlling the user interface and

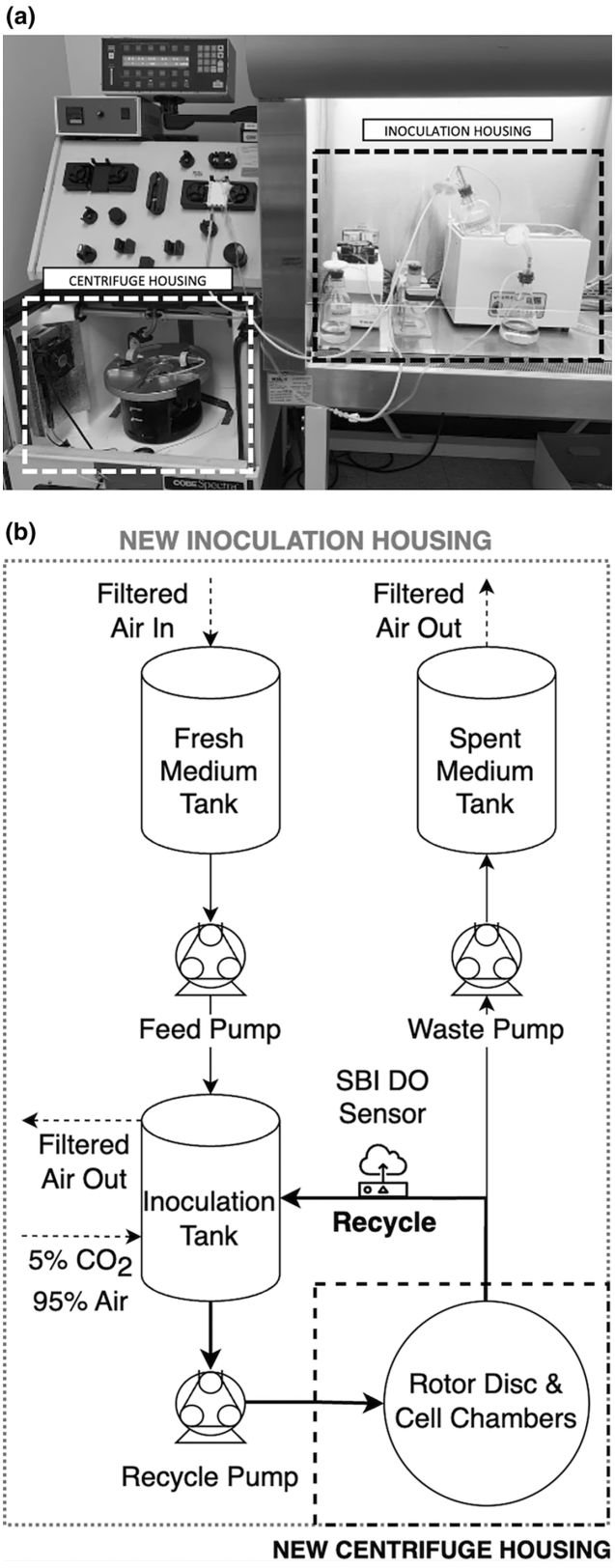

FIGURE 1 (a) The modified-COBE® centrifugal bioreactor (CBR) not operating with the front protective panel pulled down for photographing. Tubing connections to the inoculation tank are made outside of the biosafety cabinet. (b) The CBR process flow diagram with dashed lines and corresponding labels indicating where portions of the system are housed.

centrifuge. Electronic wiring was routed through guarded raceways to DIN rail wiring blade arrays and connected to corresponding control units, mounted on two outward-facing 3 mm aluminum panels within one bay of the framework, arranged to form an easy-to-access electronic interface.

2.2 | Culture chamber design for high-density cell maintenance

The CBR is a perfusion bioreactor, where the balance of centrifugal and fluid forces acts as the cell retention mechanism to maintain high cell densities in the reactor chamber rather than the use of membrane filters, which are prone to fouling, and where replacing filters once they foul is an expensive and invasive process that can introduce contamination.[18,19] The ability to rapidly expand high-density cultures is necessary for cell-based therapies because of the cell requirements for treatment; the number of cells needed varies across patients but can reach up to 2×10^8 T cells per infusion.[20] Past studies by our group expanding hybridoma cell lines with a previous model of the CBR have proven its ability to reach viable cell densities on the order of 10^8 cells/mL.[13] In addition to the cell retention mechanism, the cells are continuously, uniformly refreshed with fresh medium and nutrients, which is a key factor in maintaining exponential growth of the cells.

Various sources and protocols suggest not exceeding a relative centrifugal force (RCF) of 300g for pelleting and washing mammalian cell cultures.[21] Although 300g is a limit to consider for future CBR builds, the prototype presented in this work has a rotor disc radius of 7.5 cm and, by design, cannot exceed 1800 rpm, resulting in an RCF of 141g at the cell chamber's furthest point from the center of the rotor disc. To determine the maximum cell capacity in the chamber, the cell bed was modeled starting with packing densities for hard spheres[22] while incorporating the fact that cells are compressible or deformable by nature, as outlined in previous work from our group[23]; however, there is a critical cell density to consider, that of human tissue, which reaches values up to 3×10^9 cells/mL and serves as our absolute upper limit.[24] In practice, though, a much lower density than human tissue must be selected, otherwise the interstitial medium velocity required to sustain the cells would be so high as to induce washout of the cells. Part of this work is to determine a packing density or overall void space for modeling purposes to obtain a practical maximum cell capacity in the reactor chamber and design a reactor shape which will allow a uniform cell density from entrance to exit.

In the case that T cell growth rates may be reduced in dynamic bioreactor systems due to nonuniform mixing as suggested by other work,[25,26] we can compare the forces acting on the cells and fluid environment between the Xuri™ W25—a disposable bag technology—and the CBR. In 2019, Zhan et al. studied fluid behavior in a rocking system similar to the Xuri™ W25 and found that while the rocking mechanism promotes higher fluid velocities, the culture remains nonuniform because of the bag-orientation.[27] The CBR, however, acts in a similar manner to a fluidized bed reactor (FBR) as shown in Figure 2, where the centrifugal force on the CBR replaces what

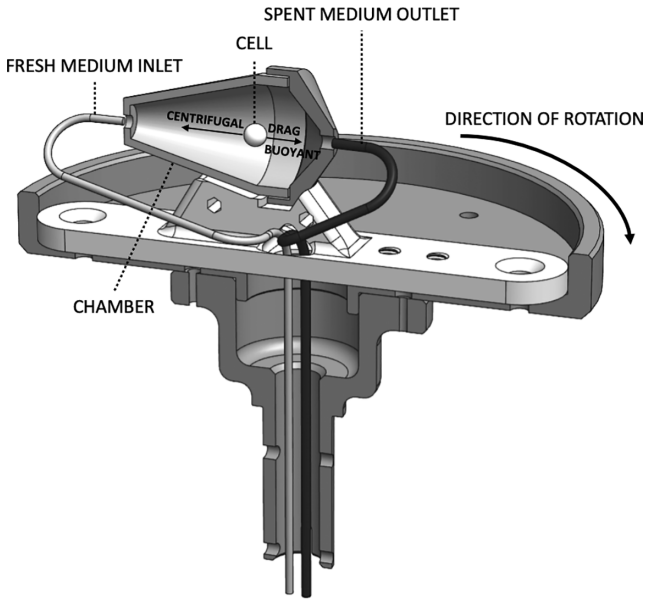

FIGURE 2 Centrifugal bioreactor rotor disc schematic and forces acting on an individual cell suspended in the chamber.

would be gravitational force in an FBR. Previous work on flow profile visualization of the CBR with cells in the chamber shows the presence of cells disrupts the Coriolis forces and result in a uniform flow of medium that suspends the cells within the centrifugal force field.[23,28]

While there are many different models that can be used to predict dense cell settling velocities, v_{cell}, we chose a relationship developed by Maude and Whitmore[29] to adjust settling velocity, as shown in Equation (1), to add an empirically derived correction term to account for the effects of population densities on apparent void space, $\varepsilon^{4.6}$, and include an overall suspension density, $\overline{\rho}_{susp}$. The angular acceleration, ω^2, and rotor disc radius, r_{rotor}, take the place of what would be gravitational force.

$$v_{cell} = \frac{r_{rotor}\omega^2 {d_{cell}}^2}{18\eta}\left(\rho_{cell} - \overline{\rho}_{susp}\right)\varepsilon^{4.6}. \quad (1)$$

2.3 | Identification, development, and validation of a CD8 cytotoxic T cell line for modeling growth and functionality for immunotherapy

To determine the efficacy of the CBR for immunotherapy, we looked for an effector target cell combination that would address some of the current challenges in study of CD8 CTL expansion. The first is the need for a constant source of a genetically identical target cell to study functional activity of CD8 CTLs. The second is the need for a constant source of a lineage of CD8 CTLs that can be expanded in a CBR to study factors that affect stability and functionality. We adapted a culture system developed to study the immune response to protozoan parasite *Theileria parva* to develop an effector target cell combination for use with the CBR.

T. parva is a protozoan parasite that causes East Coast Fever in Africa, a fatal disease in cattle, especially in European breeds of cattle—ticks are the intermediary host. African Cape buffalo (*Syncerus caffer*) is the main carrier of ticks infected with *T. parva*. They have developed resistance to the parasite and are the source of infected ticks. After transmission to cattle, the parasite infects T and B lymphocytes and synchronizes replication with replication of the infected cell. If untreated, the infected lymphocytes proliferate and cause inflammation in the lungs and death.[30] When treated with an antibiotic at the time of experimental exposure, the rate of replication is slowed allowing for development of CD8 CTLs that control the infection. A vaccination protocol was developed, using infection and treatment with an antibiotic as a method (ITM) to protect cattle from Theileriosis. Of interest to the present project, parasite infected cells are able to proliferate in vitro and serve as a constant source of autologous target cells to study the functional activity of CTLs.[31] Vaccinated cattle that survive infection can be used as an autologous source of CD8 CTLs.

Peripheral blood mononuclear cells (PBMCs) were isolated from one steer vaccinated with *T. parva* and stimulated with irradiated autologous cells infected with *T. parva* as described by Elnaggar et al.[32] After 6 days of culture the PBMCs were collected and subjected to density gradient centrifugation to remove dead cells. Rat anti-mouse IgG2a+b magnetic microbeads (Miltenyi Biotec, Waltham, MA, USA) were used to isolate CD4 and CD8 T cells labeled with anti-CD4 and anti-CD8 monoclonal antibodies. The cell preparation was subjected to another round of stimulation with irradiated *T. parva* infected cells. Following density gradient centrifugation, Rat anti-mouse IgG2a+b magnetic microbeads were used to remove CD4 T cells as described. The remaining CD8 T cells were expanded in medium containing bovine interleukin 2 (IL-2) (10 ng/mL, Kingfisher, USA). Flow cytometry was used to verify the phenotypes present in the culture, confirming a predominantly CD8 cell line.

2.4 | Batch experiments to model culture conditions required for maintaining exponential growth in the CBR

2.4.1 | Identifying kinetic growth parameters

To determine the Monod constant (K_m) and maximum specific growth rate (μ_{max}), cells were expanded in full expansion medium prepared at concentrations ranging from 2 to 225 mg/dL of glucose. Varied glucose concentrations were obtained by first determining the glucose concentration of the calf bovine serum (CBS) batch being used, as this value varies from 85 to 95 mg/dL between lots, then adding low percentages of CBS from 2% to 10% for the lower glucose concentrations then additional D-glucose at 200 g/L (Gibco) as necessary in addition to 10% CBS for higher glucose concentrations. Glucose concentrations of the stock solutions were checked with an Accu-Chek blood glucose meter before adding cells, and actual concentrations were reflected in the results if they varied from the intended

concentration. The Accu-Chek blood glucose meter cannot read glucose concentrations below 20 mg/dL, and it is assumed the lower glucose concentrations were the intended values. Each glucose concentration was tested in quadruplicate in 12-well culture plates with a seeding density of 5×10^4 viable cells/mL, incubated at standard culture conditions of 37°C and 5% CO_2, and counted every 24 h for 7 days or until cell growth plateaued—the initial cell concentration is kept low to mitigate inhibitory metabolite effects. Cell concentrations and viabilities were determined by manually counting using Trypan Blue Solution, 0.4% (Gibco). The medium recipe used for this growth experiment is glucose-free 2.05 mM L-Glutamine RPMI 1640 medium (Gibco) supplemented with 2%–10% CBS, 10 ng/mL Bovine IL-2, 100 U/mL Penicillin–Streptomycin, 1 mM HEPES buffer, and 55 μM 2-mercapto-ethanol. Results from the seven-day study were then used to produce linearized growth plots and observe growth rates with respect to glucose concentration.[33] Rather than interpolating to find K_M from the x-axis point at which $\mu = ½\ \mu_{max}$, kinetic parameters were determined from four replicate experiments with Hanes-Woolf/Langmuir plots, which minimize distortions in experimental error at the lower glucose concentrations.[33]

Critical lactate and ammonium concentrations were assessed by testing six concentrations of lactate from 0 to 16 mg/mL and six concentrations ammonium from 0 to 25 mM in quadruplicate with a seeding density of 1×10^5 viable cells/mL—ammonium and lactate concentrations were tested separately. Our complete medium recipe is similar to that used for the growth rate experiments; however, the RPMI used is not glucose-free, containing 200 mg/dL glucose, and is supplemented with 2 mM GlutaMAX™ rather than pre-existing 2.05 mM L-Glutamine. Cells were maintained at standard incubator conditions and counted every 24 h, as previously outlined in Section 2.2 at a dilution factor of 5, over a 7-day period to determine the concentrations of inhibitory metabolites that cause the cells to have a specific growth rate of 0 h^{-1}, that is, cells appear to be growing at the same rate as they are dying based on cell counts.

Lactate, ammonium, and glucose yield coefficients (Y_i, where $i = G$, A, or L) were determined by expanding quadruplicates of a single culture under standard culture conditions with variable seeding densities depending on the length of the experiment. For one experiment, cells were seeded at low density, 1×10^5 viable cells/mL, and counted every 24 h over 7 days, and for a separate experiment, cells were seeded at high density, 1×10^6 viable cells/mL, and counted every 12 h over 2 days. After every count, 150 μL samples were taken from each well to be frozen for end-of-study substrate and metabolite assays. Concentrations of glucose, lactate, and ammonium were determined using the blood glucose meter previously mentioned and enzymatic assay kits (AAT Bioquest) with spectrophotometric readings taken on a BioTek Gen5 microplate reader. Glucose, ammonium, lactate, and cell concentrations were plotted over time to observe trends and calculations were conducted to determine glucose consumption or ammonium and lactate production with respect to cell concentration. Instantaneous yields were determined from concentration changes between each day, and overall yields were determined from concentration changes from the beginning to the end of the entire study.

2.4.2 | Oxygen consumption rate

Oxygen consumption rate (OCR) experiments were conducted and compared to literature values to determine if higher recycle rates through our oxygenator are required to keep DO at sufficient levels to maintain growth in the CBR. OCR experiments were conducted by expanding a CTL culture over 5.17 h in a 50-mL Erlenmeyer flask with the culture medium completely sealed from the environment, that is, no air in the headspace. To ensure good mixing and 37°C in the culture, the flask contained a stir bar and sat on a magnetic hot plate over the course of the experiment. DO was measured with a portable oxygen meter (Ohaus ST300D) at the beginning and end of the experiment, $t = 0$ h and $t = 5.17$ h. Cells were counted manually when DO measurements were taken. Because oxygen consumed and the number of cells in the culture both change with time, we determined the change in DO and set that equal to an integral of OCR times an expression for the number of cells with respect to time. Integration and rearrangement for OCR results in Equation (2).

$$\mathrm{OCR} = \frac{\mu(\mathrm{DO} - \mathrm{DO}_0)}{C_{C0}(e^{\mu t} - e^{\mu t_0})}. \tag{2}$$

2.5 | Modeling and testing optimized CTL growth in the CBR

2.5.1 | Kinetic growth models

To predict cell growth over time with respect to inhibitory metabolites and optimize expansion in the CBR, we use a form of Han and Levenspiel's extended Monod kinetics, where the effects of inhibitory metabolites of interest are incorporated into the generalized Monod equation.[13,34]

$$\frac{dC_{\mathrm{Cell}}}{dt} = \frac{\mu_{\max} C_G}{C_G + K_M}\left(1 - \frac{C_A}{C_{A\_\max}}\right)^m \left(1 - \frac{C_L}{C_{L\_\max}}\right)^n C_{\mathrm{Cell}}, \tag{3}$$

$$D' = \frac{Q_R}{V_C}, \tag{4}$$

$$C_{iF} = \frac{C_{i0}Q_F + C_{i,n-1}(Q_R - Q_W)}{Q_R}, \tag{5}$$

$$\frac{dC_i}{dt} = D'(C_{iF} - C_i) + Y_i\left(\frac{dC_{\mathrm{Cell}}}{dt}\right). \tag{6}$$

The concentration of cells, glucose, lactate, and ammonium are represented by C_{Cell}, C_G, C_L, and C_A, respectively. Equation (3)

represents the overall growth rate of cells over time, assuming a well mixed CBR chamber, with respect to the effects of inhibitory metabolites, lactate, and ammonium, and empirically determined orders of inhibition, superscripts n and m. C_{L_max} and C_{A_max} represent critical lactate and ammonium concentrations, which are concentrations of these metabolites that will cause the observable cell growth rate to be zero. Key assumptions are made to reduce the kinetic growth equations from that of Han and Levenspiel's work and other generalized Monod growth models. We note, since the CBR is run in perfusion mode, cells are always maintained, and Equation (3) contains no terms to account for infusion or removal of cells. It is also assumed that C_G will always be significantly greater than the Monod constant, K_m, 10 times greater for modeling purposes, since we will be increasing the fresh feed rate into the CBR, or providing a high concentration glucose makeup stream, during expansion to avoid the lack of this energy source for cell growth, making K_m negligible, and canceling out the C_G terms in the numerator and denominator, or in other words operating at the maximum specific growth rate as far as glucose is concerned.

Because the cells are our product of interest and grow while retained in a chamber, we have two separate dilution rates to consider: the overall dilution rate, D, of fresh medium into the total recycle volume and the dilution rate of the recycled medium flowing into the reactor chamber, D', shown in Equation (4). Equation (5) is the concentration of either substrate or metabolites, C_{iF}, where $i = G$, A, or L, that is fed into the reactor chamber, which are weighted average concentrations of substrate or metabolites from the fresh feed and recycled medium. Equations (4) and (5) are then substituted into Equation (6), which represents the change in concentration over time of glucose substrate or lactate and ammonium metabolites, related to cell growth through respective yield coefficients, Y_i. For the purposes of this article, we assume glucose consumption is predominately attributed to growth rather than the addition of a maintenance term, as described by Dimeloe et al. for rapidly proliferating T cells.[35]

2.5.2 | Bioreactor operation

Once kinetic parameters were determined, we used the model to predict fresh medium feeding rates required to maintain glucose substrate at concentrations required for optimal cell growth. A few scenarios modeled include: (1) feeding rates required if the user were to increase the flow rate manually every 24 h, (2) use of an automated pump that would increase the fresh feed rate continuously once the glucose concentration drops to its critical value, and (3) high-concentration glucose spiking of the CBR in continuous recycle with no fresh feed or waste leaving the system. We then modeled the CBR as a plug flow reactor (PFR) to predict substrate and metabolite changes over a single pass of fresh medium, allowing us to determine the maximum cell density the chamber can sustain. Because the CBR can act as a PFR or continuous stirred tank reactor (CSTR) depending on use of recycle,[12] we compared PFR and CSTR volumes required to consume from 1% to 99% of the initial glucose at the maximum sustainable cell density to establish a substrate concentration range at which the CBR is most efficient. The goal was to optimize CBR operation by minimizing loss of glucose, inhibitory metabolite concentrations, and the time it takes to produce enough viable cells.

Because we intended to iterate on the CBR prototype design, we also defined a function to create the ideal CBR chamber shape that would balance cells at any point of the chamber without needing to change the recycle balancing flow rate—mitigating user error. To determine the ideal chamber shapes, we solved for the chamber radius, r_c, by matching the balancing fluid velocity with decreases in centrifugal force as flow proceeds inwardly shown in Equation (7).

$$r_c = \frac{3}{\omega d_{\text{cell}} \varepsilon^{3.3}} \sqrt{\frac{2\eta Q_R}{(\rho_{\text{cell}} - \rho_{\text{fluid}})R}}. \tag{7}$$

All modeling aspects were compared to data expanding CTLs over a 120 h experiment in the CBR prototype. The CBR was cleaned prior to the experiment by recycling 75 mL of 70% ethanol-water mixture over 12 h with UV turned on for 4 h. The ethanol-water mixture was then removed via the waste stream and replaced with 75 mL basal RPMI for 1 h to remove remaining trace amounts of the ethanol-water mixture. During the basal RPMI recycle, the heating controls were started, and the air pump feeding gas from a nearby incubator into the inoculation tank was turned on. The basal RPMI was then replaced by supplemented RPMI for culture and the CBR was inoculated with 1.0×10^7 viable CTLs to start the experiment. Balancing recycle rates and fresh medium feeding rates were chosen based on the kinetic growth model. Quadruplicate 0.5 mL samples were taken every 24 h from the inoculation tank for cell counts and glucose checks. Once all data were collected, it was plotted against the kinetic model to determine percent agreement.

3 | RESULTS

3.1 | Kinetic growth parameters

As anticipated, batch culture experiments showed a rapid increase in specific growth rate with increasing glucose concentrations as it approached its maximum value, resulting in a low Monod constant, that is, glucose concentration needed to operate at half the maximum specific growth rate. Between glucose concentrations 2 and 16 mg/dL, the specific growth rate increases 1.8-fold from 0.012 to 0.022 h^{-1}, approaching an average value of 0.023 ± 0.002 h^{-1} between 16 and 225 mg/dL glucose. Hanes-Woolf linearization results in a μ_{max} and K_M across quadruplicate samples of 0.024 ± 0.001 h^{-1} and 2.5 ± 0.6 mg/dL, respectively with an R^2 of 0.995, translating to a doubling time of 28 h. The specific growth rates from the experimental data were within 5% agreement of the Hanes-Woolf plot for concentrations. The culture environment must be maintained at a glucose concentration no lower than 50 mg/dL, 20 times greater than K_M, for the cells to grow within 5% of μ_{max}. Therefore, for modeling purposes and bioreactor

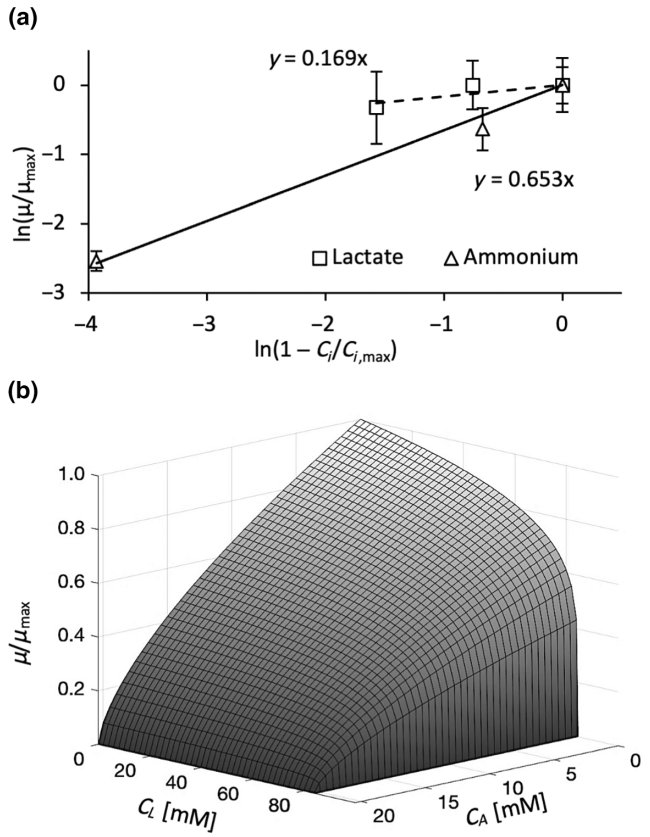

FIGURE 3 Bovine CTL growth trends over increasing metabolite concentrations. (a) Linearized kinetic model with respect to inhibitory metabolite terms to determine orders of inhibition for ammonium, *m*, and lactate, *n*. (b) Comparison of the singular and multiplicative effects of ammonium and lactate on normalized specific growth rates over increasing inhibitor concentration.

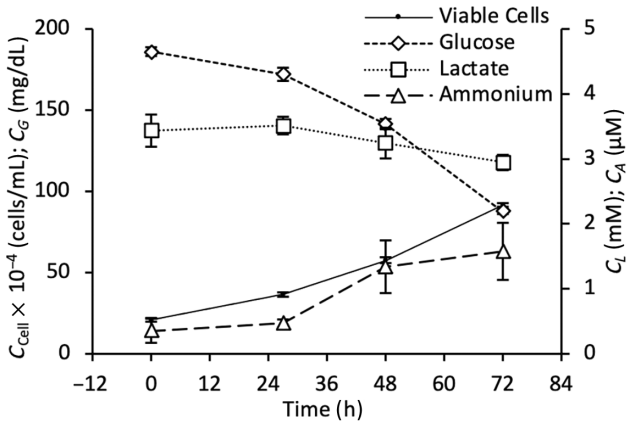

FIGURE 4 Viable cell density, substrate, and metabolite concentrations over a three-day expansion of bovine cytotoxic T lymphocytes. As viable cell density increases, glucose concentration decreases and ammonium concentration increases, as expected; however, lactate concentrations decrease and may be used faster than it is produced at the present study cell densities.

operation, the glucose concentrations must be maintained above 50 mg/dL to ensure lack of glucose substrate does not inhibit cell growth.

Critical metabolite concentration batch experiments revealed that complete inhibition after one-day exposure by ammonium occurs at a lower molar concentration than for lactate at 20.4 mM and 84.6 mM, respectively. Knowing $C_{A,max}$ and $C_{L,max}$ from the cell expansion fold plots, we show the order for ammonium inhibition is much higher than that for lactate and, therefore, if they are at the same concentration, ammonium will have a much greater impact on cell growth. To do this, we linearized forms of Equation (2) holding glucose at a high and constant concentration and beginning with none of the opposing inhibitor present. Respective plots of $\ln(\mu/\mu_{max})$ versus $\ln(1 - C_i/C_{i,max})$ for both inhibitory metabolites are shown in Figure 3a, where the slopes reveal orders of inhibition m for ammonium and n for lactate in Equation (2) of 0.653 and 0.169, respectively. Because about a 4-fold higher concentration of lactate is needed to fully stagnate cell growth, shown in Figure 3b, ammonium concentration, all else being equal, is of most concern for this particular cell line. What is important now is to determine the rates of ammonium and lactate production to see which species will reach significantly inhibiting levels first.

With orders of inhibition of 0.653 and 0.169 for ammonium and lactate, respectively, we make an initial assumption that ammonium is the primary inhibitory metabolite; however, yield coefficient studies change one's thinking as lactate is produced at much faster rate than ammonium with respect to the critical concentrations. When considering collective effects of maximum inhibitor concentrations, orders of inhibition, and yield coefficients, we find that glucose consumption is of greatest concern for the CBR process. Batch culture yield coefficient experiments revealed changing values or changing consumption or production rates of glucose, lactate, and ammonium with respect to cell growth over time. Cell density, glucose, lactate, and ammonium concentrations are presented in Figure 4 as a function of time over a 72-h period. For quadruplicate batch cultures inoculated at $2.1 \pm 0.1 \times 10^5$ cells/mL, we observed a 4.4-fold increase in viable cell concentration and a μ_{max} of 0.02 h^{-1}—a value slightly lower, potentially due to being in a lag phase, yet, consistent with the 0.023 h^{-1} μ_{max} value presented in Section 4.1.

Beginning at a glucose concentration of 187 ± 3 mg/dL, consumption over 72 h reduced the concentration down to 87.6 ± 1.4—a value 45 times greater than K_m such that substrate inhibition is not an issue for this experiment. Over the course of the batch culture, ammonium began at 0.35 ± 0.18 μM and rose 4.5-fold to 1.6 ± 0.4 μM, which is not of concern as a 1.6 μM concentration reduces μ_{max} by less than 0.01% based on the previously discussed critical concentration studies. Unexpectedly, average initial lactate concentration was 3.4 ± 0.3 mM and decreased 0.86-fold to 3.0 ± 0.1 mM, suggesting the CTLs utilize lactate as part of a regulatory mechanism or at a rate faster than it is being produced.

As described by Doran[33] and observed in the present study, the yield coefficients change over time when comparing 24-h blocks across the 72-h study. The calculated instantaneous yields in comparison to the overall yield are shown in Table 1. For our overall yield, we took into account the concentration change between 24 and 72 h

Δt (h)	Glucose $\left(\frac{mg/dL}{10^6\ cells/mL}\right)$	Lactate $\left(\frac{mM}{10^6\ cells/mL}\right)$	Ammonium $\left(\frac{\mu M}{10^6\ cells/mL}\right)$
0–24	−98	1.4	0.9
24–48	−147	−1.2	4.4
48–72	−158	−0.8	1.5
24–72	−155 ± 9	−1.0 ± 0.3	2.0 ± 0.9

TABLE 1 Instantaneous yields of substrate and metabolites.

TABLE 2 Kinetic growth parameters.

Parameter	Value	Units
μ_{max}	0.024 ± 0.001	h^{-1}
K_m	2.5 ± 0.6	mg/dL
$C_{A,max}$	20.4	mM
$C_{L,max}$	84.6	mM
m	0.653	–
n	0.169	–
Y_G	−155 ± 9	$\frac{mg/dL}{10^6\ cells/mL}$
Y_A	2.0 ± 0.9	$\frac{\mu M}{10^6\ cells/mL}$
Y_L	−1.0 ± 0.3	$\frac{mM}{10^6\ cells/mL}$

rather than including the first 24 h, where the cells are acclimating to the culture environment. Yield coefficients calculated from these experiments accurately reflected the non-inhibited values for cell culture. In the following modeling studies, it is assumed the average yield coefficient values are retained if cells were to undergo inhibited growth in the presence of lactate and ammonium metabolites.

With the full spectrum of kinetic parameters shown in Table 2, modeling of the process from inoculation to harvesting of CTLs can be accomplished. Based on overall yield, ammonium is produced at less than a fraction of a percent of its critical concentration every 1×10^6 cells/mL increase in density; however, the question remains whether ammonium concentration reaches inhibiting levels at all before cells are removed from the CBR. This is determinable by process modeling and validated by continuous flow monitoring.

3.2 | The CBR prototype

The final build of the CBR prototype requires 0.28 m^3 of space and has a centrifugal range of 0–1800 rpm for a 14 cm rotor disc on which the cell chamber sits (Figure 5). The small footprint is appropriate for use on standard laboratory benches and is small enough to transport through single-panel doors. During operation, we found medium evaporation was an issue since the inoculation tank has an air headspace. An open water tray with germicidal fluid was placed in the inoculation housing area of the CBR, similar to water trays in static culture incubators, to humidify the enclosure and mitigate medium evaporation. The electronic units controlling the user interface and centrifuge are housed in the far-right compartment hidden by the dark (blue) panel in Figure 5.

Initial build cost through the Washington State University (WSU) Machine Shop for materials and labor was $23,700, taking 310 work hours to build. Although we expect to make more changes to the prototype with each iteration, the reduced size and simplified user interface are steppingstones to increase market potential of the CBR for cancer research centers, hospitals, and biopharmaceutical companies.

3.3 | Experimental data expanding CTLs in the CBR

Experimental results strongly support our hypothesis that the CBR is useful for producing clinically relevant numbers of CTLs. Figure 6a depicts a 120-h study in the CBR where we expand 1×10^7 viable CTLs to 1.2×10^8 viable CTLs. The recycle rate was maintained at 1.1 mL/min to balance the cells in the CBR chamber and provide sufficient DO in the inoculation tank, while the fresh feed rate was increased from 0.016 to 0.044 mL/min in 0.007 mL/min increments each day to maintain adequate glucose levels. Moreover, experimental data agreed with predicted cell numbers to within an average of 95% when assuming a μ_{max} of 0.0223 h^{-1}, which is at the lower end of the experimental error. DO data collected with the SBI fiber optic report 5% higher, on average, than values predicted with our empirically derived OCR—Figure 6a shows SBI DO values deviate from the model past 72 h. During operation, despite use of a humidifying open water tank within the inoculation compartment, approximately 10 mL/day of medium evaporated from the inoculation tank. We attribute evaporation to the relatively high 37°C environment and deviation from 100% humidity. When incorporating a constant evaporation rate of 0.007 mL/min into the model, results show an apparent increase in glucose concentration such that data and the model agree within 1% agreement on average. Initial glucose concentration in the feed was determined to be 187 mg/dL for this experiment and used in the model.

At the end of the expansion study, the CTLs were harvested from the recycle loop and immediately labeled for flow cytometry to determine phenotypes present in the culture. Cells were labeled with anti-CD4- and anti-CD8-specific antibodies and flow cytometry was used to confirm the phenotype of the cells. As shown in the dot plot in Figure 6b, labeling with anti-CD8 antibodies resulted in a shift toward the right. All cells had been labeled with both CD8- and CD4-specific antibodies, so this shift indicates the detection of CD8 cells, with fluorescence specific to CD8 co-receptors detected from light scattering. The flow cytometry determined that the cell population was 95% CD8 positive. The dot plot in Figure 6c shows that there was no shift

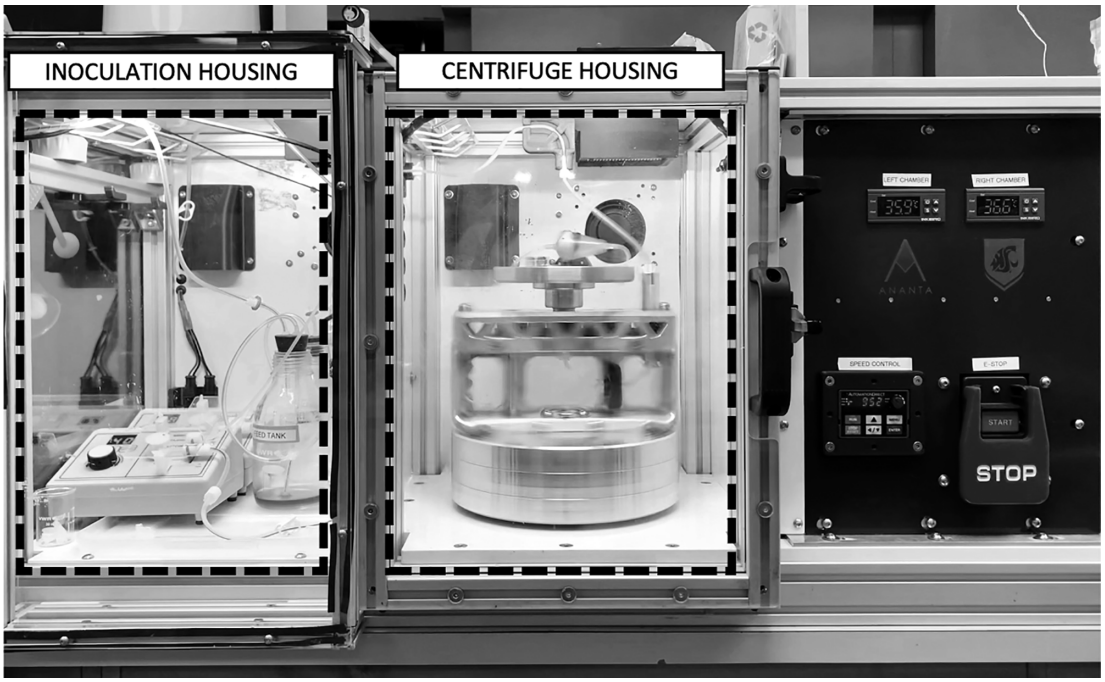

FIGURE 5 The self-contained centrifugal bioreactor prototype on a standard lab bench.

to the right of cells labeled with anti-CD4, indicating that there was no fluorescence specific to CD4 co-receptors detected on the cells, and confirming that nearly all the cells were CD4 negative. The flow cytometric assays confirm the CTLs maintained their CD8 phenotype, that is, killing ability, over the course of the expansion in the CBR.

3.4 | CTL growth predictions in the CBR

To grow at least 2×10^8 cells, the maximum dosage of T cells for a single immunotherapy infusion,[20] we devised a process that will take 4.4 days of operation in the CBR starting with 2×10^7 cells. To obtain this with the CBR as is, the user can increase the fresh feed rate daily as shown in Figure 7a to prevent glucose levels from dropping below 49.4 mg/dL, that is, 20 times K_M, before the next time the user checks the CBR.

Feed rates for each consecutive day were 0.007, 0.019, 0.035, 0.061, and 0.107 mL/min with a constant recycle rate, Q_R, of 1.0 mL/min, requiring a total of 263 mL fresh medium. Under these conditions, lactate and ammonium do not reach concentrations high enough to inhibit the specific growth rate by more than 5%, when considering both individual and multiplicative inhibition terms. DO levels were maintained over the course of the expansion based on an OCR of 1.9×10^{-11} mmol O_2/cell × h determined experimentally for our CTLs. The Q_R chosen provides a drag force at the centroid of the suspension sufficient to maintain a suspension density of 2.81×10^7 cell/mL. Based on previously reported modeling,[29] Q_R was calculated by multiplying the cell settling velocity in Equation (1) by the cross-sectional area for flow and the effective porosity, ε.

Another scenario shown in Figure 7b is if the fresh feed pump rate were automated to increase continuously over time to maintain $20 \times K_M$ once the glucose concentration drops to that value. The fresh feed rate, Q_F, was calculated by setting the change in glucose concentration to zero and solving for Q_F, using Equations (3)–(6) with the result shown in Equation (8). The same initial cell number and recycle rate were used in Figure 7b as portrayed in Figure 7a; however, we find that 233 mL of fresh medium is required to expand 2×10^8 cells, 30 mL less than if the user were to increase the feed rate once a day manually.

$$Q_F = \frac{-Y_G V_C \left(\frac{\partial C_{Cell}}{\partial t}\right)}{C_{G0} - C_{Gn}} \left[\frac{\text{mL}}{\text{min}}\right]. \tag{8}$$

If glucose was the only substrate pertinent to growth, we can further minimize fresh medium requirements by spiking the feed glucose concentration to its initial concentration, 180 mg/dL, as frequently as needed to keep existing glucose above $20 \times K_M$ rather than continuously increasing the fresh medium dilution rate. Figure 7c shows nine glucose spikes, with increasing frequency, are necessary over the course of a 3-day expansion if one were operating the CBR with no fresh feed entering or spent medium leaving the system, maintaining a recycle rate of 1.0 mL/min, shown to maintain adequate DO levels due to gas exchange in the inoculation tank. This scenario only requires 42 mL of fresh medium. We note identifying other critical growth factors aside from glucose and introducing them at high concentrations into the inoculation tank may be necessary.

To determine the maximum cell density the CBR can sustain, the chamber is modeled as a PFR to observe substrate, metabolite, and DO changes over a single pass of fresh medium in Figure 8. Previous tracer studies show without recycle there is little dispersion and PFR-

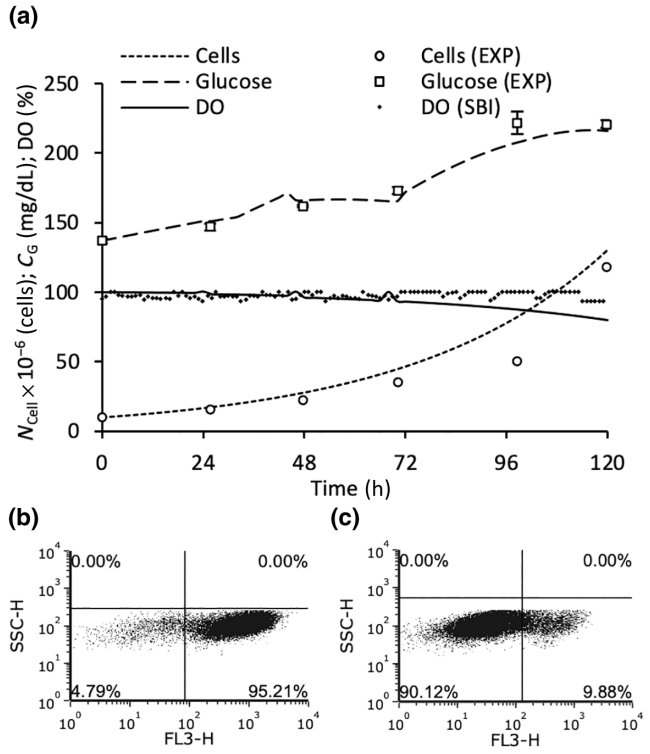

FIGURE 6 Experimental data culturing bovine cytotoxic T lymphocyte (CTL) in the centrifugal bioreactor (CBR) prototype. (a) Expanding 1.00×10^6 to 1.2×10^8 viable cells over 120 h in comparison to model predictions. Cell counts and glucose samples were taken every 24 h. SBI dissolved oxygen (DO) sensors collected data every 10 min; however, only points from the 1-h increments are reported. Cells grew at the lower end but within error of the maximum specific growth rate. The model was updated to account for medium evaporation in the inoculation tank, affecting the glucose concentrations. (b) Flow cytometry results of CTLs harvested from the CBR labeled with anti-CD8 and (c) anti-CD4 confirming 95% of the cells were CD8.

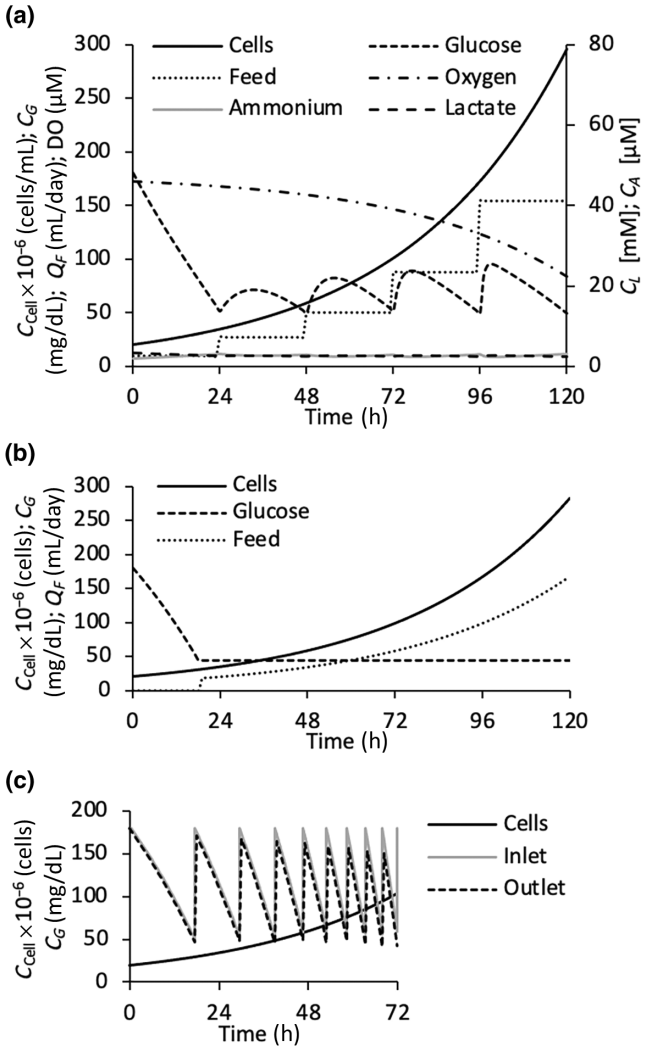

FIGURE 7 Using kinetic models to maintain substrate levels in the centrifugal bioreactor (CBR) during different operating scenarios. (a) Modeling 2×10^7 cells in the CBR at a recycle rate of 1.0 mL/min and increasing fresh feed once every 24 h at rates 0.007, 0.019, 0.035, 0.061, and 0.107 mL/min to assure that glucose never falls below $20 \times K_M$. It is noted that dissolved oxygen (DO) in this case does not deplete, as the recycle is saturated with DO. (b) An example of how an automated pump could increase the fresh feed rate continuously to maintain $20 \times K_M$ once the glucose concentration drops to that value. (c) Expansion over 3 days in continuous recycle at 1.0 mL/min with no fresh feed or waste leaving the system showing the frequency of substrate spiking needed to maintain glucose levels exiting the reactor chamber above $20 \times K_M$ to prevent growth limitation.

like behavior dominates.[12] Visual observations also made it appear as though the cell density with respect to volume remains constant as cells grow; the bed increases in height in the direction of fluid flow, similar to an upright fluidized bed column.

For our calculations, we selected a cell density that would fill the space in the chamber up to the greatest cross-sectional area and calculated the appropriate balancing flow rate, in this case the fresh feed rate, Q_F. This must be decreased with increasing cell density and affects the rate at which DO is replenished. By modeling various cell densities, we find the maximum cell density the reactor can sustain, at the centroid, is 5.53×10^7 cells/mL with a corresponding Q_F of 0.67 mL/min at 1000 RPM, with DO being the limiting factor.

3.5 | Reactor sizing

Analyses revealed the same volume requirements for a PFR and CSTR until glucose concentrations approach 50 mg/dL, approximately $20 \times K_M$, after which PFR volume requirements are significantly lower. This is because glucose levels throughout a CSTR were too low to maintain maximum specific growth rate, while those in the PFR only became that low near the exit of the CBR. Models for the PFR and CSTR appear in Equations (9) and (10). Respective volumes plotted in Figure 9 are within 5% agreement until 74% of the initial glucose is consumed, then volumes deviate significantly afterward. For example, if operation resulted in consumption of 99% of the glucose,

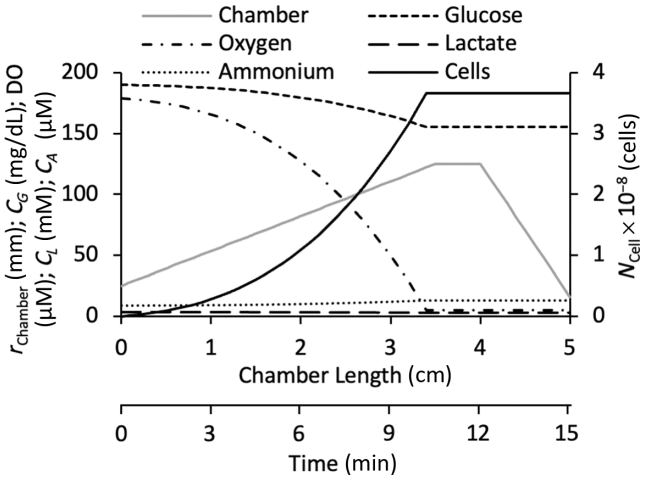

FIGURE 8 Modeling the centrifugal bioreactor as a plug flow reactor over a single pass of fresh medium to predict substrate and metabolite changes. The maximum number of cells the chamber can sustain is 5.53×10^7 cells/mL at a corresponding balancing flow rate of 0.67 mL/min and 1000 RPM before dissolved oxygen is completely depleted after a single pass.

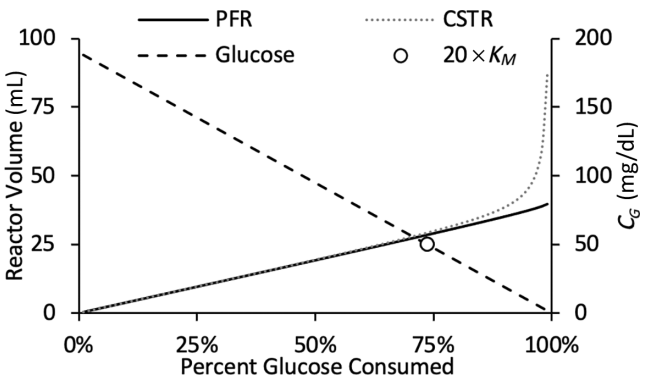

FIGURE 9 Comparing plug flow reactor (PFR) and continuous stirred tank reactor (CSTR) volumes required to consume 1%–99% of the initial glucose in a single pass at the maximum sustainable cell culture density of 5.53×10^7 cells/mL with a balancing flow rate of 0.67 mL/min.

the CSTR volume required would be more than double that of the PFR to obtain the same conversion.

$$V_{PFR} = \frac{Q_F(C_{G0}X + K_M \ln(1-X))}{\mu_{max} C_{cell} Y_G}, \quad (9)$$

$$V_{CSTR} = \frac{Q_F X(C_{G0}(1-X) + K_M)}{\mu_{max} C_{cell} Y_G (1-X)}. \quad (10)$$

For our modeling purposes based on the current CBR set-up, we were interested in manipulating the balancing inward fluid velocity entering the cell chamber with the net cell settling velocity due to the centrifugal force after adjusting for buoyant forces. We considered cases where the chamber is filled with 2×10^8 cells, the maximum

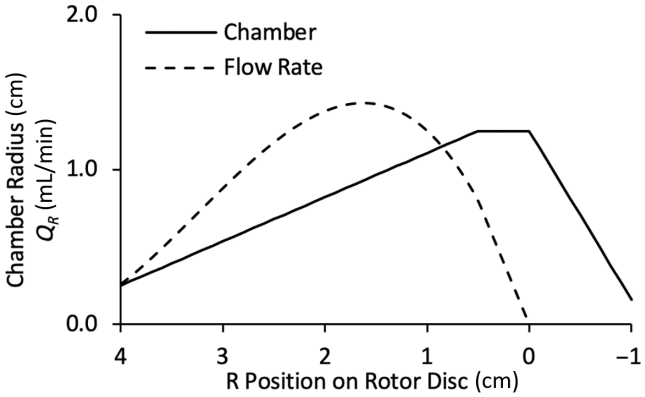

FIGURE 10 Recycle flow rates required to balance 2.82×10^7 cell/mL, i.e., an effective porosity, ε, *of* 0.975, in the current centrifugal bioreactor chamber design rotating at 1000 rpm. Positive values of R represent regions of increasing centrifugal force opposed to the fluid flow direction, whereas negative values are where centrifugal force is in the same direction as fluid force. $R = 0$ is at the chamber's greatest cross-sectional area before tapering inward toward the exit port.

number of Yescarta® T cells allowed for transfusion into an adult patient, at a density of 2.82×10^7 cell/mL occupying 7.1 mL of the chamber, that is, the space before reaching the maximum cross-sectional area, $A_{x,max}$. Since recycle is used to preserve serum components and promote oxygenation, the resultant fluid velocity is calculated by taking the recycle flow rate, Q_R, divided by the product of the cross-sectional area normal to the flow and the porosity ε. Since flow proceeds radially inward, the centrifugal force decreases linearly with distance, and the CBR taper would ideally be designed so inward fluid velocity gradually reduces to compensate for decreasing centrifugal force. Figure 10 is based on how the reactor chamber currently sits on the rotor disc, and for future chamber designs, the entire chamber would sit past the center axis, so the fluid force is always opposing the centrifugal force.

Because the walls of the current CBR chamber are linear, the cell settling velocity and resulting balancing flow rate needed follow a nonlinear trend as the fluid approaches the rotor disc center as shown in Figure 10. The cells will expand up to the point of $A_{x,max}$, where any cells past this point will elute because the fluid velocity will exceed the decreasing radial centrifugal force. When modeling the centrifuge at 1000 rpm, we found the counterbalancing fluid flow rate to maintain cells in the chamber, in our case the recycle flow rate, Q_R, increases to a maximum until reaching position $R = 1.6$ or in other words, 1.6 cm away from the center of the rotor disc (Figure 10)—this value would change at different centrifugation rates. Distances below 1.6 cm away from the center of the rotor disc require a decreased flow rate needed to balance the cell bed, until the cells reach the center of the rotor disc, where a flow rate of 0.0 mL/day is needed to balance the cells at that point.

To determine the ideal chamber shape, we can solve for r_c in Equation (11) by matching the balancing fluid velocity with decreases in centrifugal force as flow proceeds inwardly. Figure 11a,b show

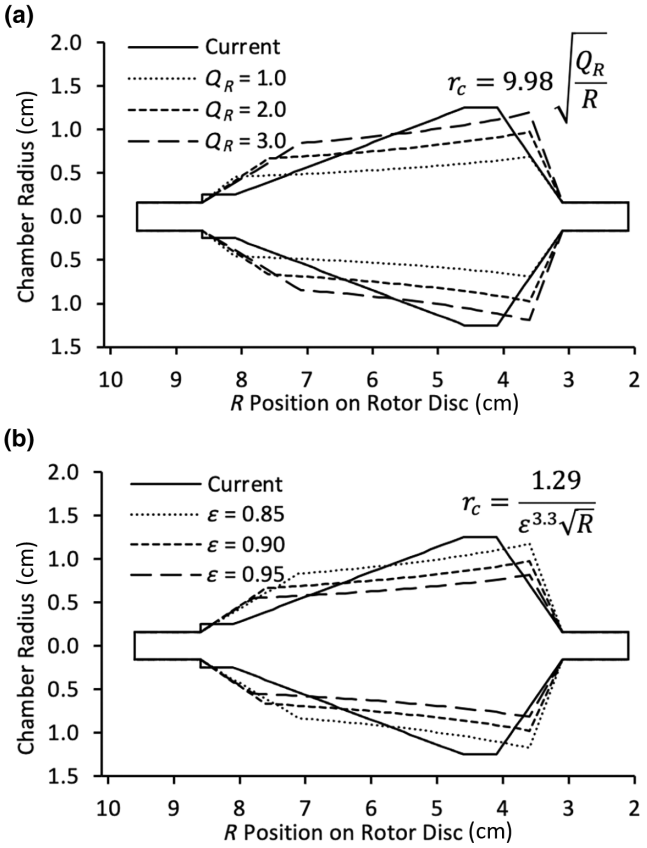

FIGURE 11 Ideal centrifugal bioreactor chamber shapes with respect to balancing flow rate or cell density. (a) Chamber shapes that will balance 1.11×10^8 cell/mL, at $\varepsilon = 0.90$, on a 30-cm rotor disc rotating at 1000 rpm. Unchanging parameters produce a chamber constant, $K_{c\varepsilon}$, of 9.98 $s^{0.5}$. Increasing recycle flow rate results in a larger ideal chamber radius. Tapers at the end are representative of 1/8″ ID straight fittings. (b) In another scenario, we maintain a recycle flow rate of 2.0 mL/min and increase the effective porosity with all other parameters remaining the same. We determine a new chamber constant, K_{cQ}, of 1.29 $cm^{1.5}$, and find that increasing effective porosity results in a smaller ideal chamber radius.

idealized chamber shapes when modeling for a 30-cm-diameter rotor disc spinning at 1000 rpm and cell suspension porosity, ε, of 0.95 with Q_R as a parameter (Figure 11a), or with Q_R set to 0.1 mL/min and ε as a parameter (Figure 11b). We note r_c can be reduced to a very simple formula for a given set of conditions as shown in Equation (11) with $K_{c\varepsilon}$ and K_{cQ} as chamber constants.

$$r_c = K_{c\varepsilon}\sqrt{\frac{Q_R}{R}} \text{ or } \frac{K_{cQ}}{\varepsilon^{3.3}\sqrt{R}}. \quad (11)$$

Predictably, chamber radii requirements increase with the inverse of the half root of R and of Q_R since cross-sectional area is proportional to r_c^2 and centrifugal force varies linearly with R while flow velocity varies linearly with Q_R. Radii also vary with $1/\varepsilon^{3.3}$ because sedimentation rates decrease with $\varepsilon^{4.6}$,[29] the difference between the cell and suspension densities decreases with ε, and interstitial velocity is a function of $1/\varepsilon$ making the combined effect dependent on $\varepsilon^{6.6}$. Therefore, when considering the r_c^2 dependence on the cross-sectional area, $\varepsilon^{3.3}$ appears in the denominator.

4 | DISCUSSION

4.1 | Kinetic growth parameters

The bovine CTL μ_{max} and K_M values of 0.024 ± 0.001 h^{-1} and 2.5 ± 0.6 mg/dL, respectively, are of the same order of magnitude as those in extant literature. Yahia et al. compared kinetic parameters for mammalian cell lines, revealing that μ_{max} and glucose K_M range from 0.019 to 0.125 h^{-1} and 1.5 to 86.2 mg/dL, respectively—our CTL values of 0.024 ± 0.001 h^{-1} and 2.5 ± 0.6 mg/dL are at the lower end of both ranges found in their report.[36] Huynh et al. cultured bovine mammary alveolar T (MAC-T) cells with a doubling time of 17 h, translating to a specific growth rate of 0.041 h^{-1}.[37] The majority of CD8 T cells studies are in mouse models; De Boer et al. compared CD8 and CD4 T cell responses in vivo and found their CD8 T cells have a doubling time of 8 h, that is, a specific growth rate of 0.087 h^{-1}.[38] Schlub et al. measured doubling times for murine CD8 T cells in the lung, liver, and spleen to be 7.5, 10, and 12 h, respectively, or a specific growth rate range of 0.058 to 0.092 h^{-1}.[39] It is important to note growth rates vary across animal sources and location of cells of origin; the closest values to our bovine CTLs are Chinese Hamster Ovary (CHO) cells, with μ_{max} and glucose K_M of 0.028 h^{-1} and 1.51 mg/dL, respectively.[40]

The bovine CTLs must have access to no lower than 50 mg/dL glucose at any given time during expansion to grow at the maximum rate of 0.024 h^{-1}, a doubling time of 29.4 h, and high glucose values above 200 mg/dL become slightly inhibitory. Upon further research, glucose concentrations approaching 10 mM, or 180 mg/dL, are considered pre-diabetic, and concentrations past 10 mM would be similar to diabetic conditions in the cell culture environment.[41] Furuichi et al. studied the effects of glucose on an adherent mammalian cell line and found significantly higher proliferation of cells in low-glucose DMEM, 2 mM or 36 mg/dL glucose, than in standard-glucose DMEM, of 19 mM or 342 mg/dL, by approximately 2-fold over a 6-day expansion.[42] In comparison to our work, 50 mg/dL glucose is where the specific growth rate is just approaching, within 5% of its maximum value, and perhaps the pre-diabetic or diabetic conditions at the higher glucose concentrations of 134 and 225 mg/dL are slightly inhibitory, hence the 0.001 h^{-1} and 0.002 h^{-1} drop in growth rate from the maximum value at those points.

The critical lactate and ammonium concentrations determined for bovine CTLs, 84.6 mM and 20.4 mM, respectively, are comparable to inhibiting values for other cell lines. Barbieri et al. showed 38% less viable cells after 72 h of expanding mouse CD8 T cells in 50 mM of sodium lactate versus 20 mM.[43] In comparison to our work, 50 mM lactate is the point at which the growth rate is 14% lower than μ_{max}. As for ammonium, Feng et al. exposed primary bovine MAC-T cells to 4 mM ammonium chloride, resulting in an apoptotic cell ratio of 1.8 compared to a ratio of 0.5 for the control.[44] Although a seemingly low

concentration caused a higher apoptotic cell ratio, in relation to our work, 4 mM ammonium is the concentration at which the growth rate is 13% lower than μ_{max}.

Yield coefficient experiments result in trends and values consistent with literature that increase initially, then level off to an average value with reasonably small relative standard deviations. Our glucose yield coefficients increase from −98 to an average steady state value of $-155\ \frac{mg/dL}{10^6\ cells/mL}$, which is in reasonable agreement with those measured by Henry et al. which decreases from −180 to an average steady state value of $-109\ \frac{mg/dL}{10^6\ cells/mL}$ for rat hybridoma cells over 72 h.[45] Average ammonium and lactate yield coefficients from our study are $2.0\ \frac{\mu M}{10^6\ cells/mL}$ and $-1.0\ \frac{mM}{10^6\ cells/mL}$, respectively; whereas Henry et al. report values for ammonium trending downward from 1.7 to 0.6 $\frac{mM}{10^6\ cells/mL}$ and lactate production yield from 10.0 to 8.6 $\frac{mM}{10^6\ cells/mL}$. The leveling trends are consistent with our findings that yield coefficients in the first 24 h trend toward a pseudo-steady-state value as cells acclimate to the culture environment. Though initially unanticipated, our studies suggest CTLs are utilizing lactate. Recent mechanistic experiments conducted by Wen et al. reveal a regulatory mechanism in which lactate contributes to enhanced production of IL-2 cytokine in activated T cells,[46] hence the deviation in lactate yield from our studies compared to those conducted with the rat hybridoma.

4.2 | Optimized operating parameters

By modeling various scenarios for CTL production, we revealed CBR manufacturing limits and avenues for improving the prototype. By comparing PFR and CSTR behavior, we found substrate levels must be maintained above $20 \times K_M$ to expand cells most efficiently in a CSTR. Prior work shows the CBR portrays CSTR behavior when recycle is introduced; otherwise, the CBR behaves as a PFR.[12] Because a higher flow rate is needed to suspend the cells than to maintain a culture environment suitable for growth, the CBR must operate with recycle and will behave as a CSTR in practice. This validates the importance of maintaining glucose levels above $20 \times K_M$.

When we omit recycle and model a single pass of fresh medium through the CBR chamber to sustain 5.5×10^7 cells/mL, DO is nearly depleted because the oxygen level in the fresh medium is not sufficient to keep pace with the OCR. At high cell densities, the balancing flow rate must be lower to properly retain the tightly packed cells in the chamber, increasing the residence time of the medium, therefore, making DO our limiting factor and 5.5×10^7 cells/mL the maximum cell density we can sustain. Glucose usage is modeled by omitting the maintenance term and assuming the yield coefficient is only associated with cell growth–this assumption is vetted by experimental evidence from Henry et al. who show glucose maintenance demands are below $1 \times 10^{-11}\ \frac{mmol}{cell \cdot h}$, that is, one tenth the value of that required for cell growth of mammalian cell lines.[45] The maximum cell density the CBR can sustain, however, is 1.6-fold more dense than a high-density value of 3.5×10^7 cells/mL obtained in recent literature with a stirred tank bioreactor.[47]

4.3 | CBR modifications for future work

The present study with the CBR shows we can manufacture a clinically relevant number of CTLs; however, changes to future prototype iterations would enhance usability. By culturing in the current CBR, we produced 1.04×10^7 cells/mL, and, while not considered high density,[47] with a dual-chamber CBR at that cell density we can manufacture the maximum dosage of T cells for one infusion of Yescarta® T cell therapy.[20] To increase the maximum cell density the CBR can sustain, a higher recycle rate is needed, which must be countered by a higher centrifugal force to balance the cells. At higher Q_R and lower ε values, that is, higher cell densities, however, we become concerned about eddies forming at the medium entrance due to the larger cross-sectional area needed to balance the cells. To reduce the cross-sectional area along the entire length of the cell chamber and retain higher cell densities, larger diameter rotors are required. With a 30-cm rotor disc, we could sustain 1.7×10^8 cells/mL, an order of magnitude greater than the current prototype, at a recycle flow rate of 2.0 mL/min. Because the cross-sectional area for flow along the length of the chamber was calculated from the cell settling velocity, the recycle rate would not need to be changed as the cell bed increases in height, reducing the need for user interaction and error.

We expect that use of higher quality variable-control pumps in future studies will mitigate evaporation medium loss by setting the fresh feed pump at a slightly higher rate than the waste pump. Wear and tear of the pumps and tubing altered the intended flow rate, hence not fully compensating for evaporation. A design alternative to eliminate medium evaporation is to use dual-lumen gas-permeable tubing in place of sparging the inoculation tank. One tube would contain a continuous flow of air with 5% CO_2 and the other tube medium. Additionally, while pH was not monitored or independently controlled in the present study, a future CBR prototype may include SBI's dual flow cell, which continuously monitors both DO and pH, in place of the single DO flow cell.

While the current CBR prototype is sufficient for expanding clinically relevant numbers of cells for autologous treatments, modifications to obtain higher densities may be advantageous for biopharmaceutical companies who are mass manufacturing cells for allogeneic therapies.

5 | CONCLUSIONS

Through this work, we have considered the most important design implications to biomanufacture T cells in the CBR for immunotherapy. We sought to provide data supporting that the CBR prototype can be used to expand clinically relevant numbers of CTLs, producing 1.2×10^8 cells over 5 days starting with 1.0×10^7 cells in a single 11.4-mL chamber. The experimental trends agree within 5% of predictions made from a kinetic growth model developed in this study, and inhibitory metabolites, lactate and ammonium, do not reach levels that hinder cell growth. It is recommended to keep glucose levels above $20 \times K_M$ to maintain growth within 5% of μ_{max} and most efficiently

expand CTLs without requiring a larger CBR volume. Moreover, we provide avenues for modifying the CBR for adoption by cancer centers, expanding patient-specific treatments, or for biopharmaceutical companies manufacturing allogeneic cell therapies. Innovations in both engineering and immunology provide a platform for studying the efficacy of the CBR for T cell manufacturing for cancer immunotherapy. The results bring to light the impact of interdisciplinary research in solving the increasingly complex problems our world faces, especially in health and medicine.

NOTATIONS

C_A	Ammonium concentration (mM)
$C_{A,\max}$	Critical ammonium concentration (mM)
C_{cell}	Cell density (cell/mL)
C_G	Glucose concentration (mg/dL)
C_{Gn}	Glucose concentration exiting CBR (mg/dL)
C_{C0}	Initial cell concentration (cell/mL)
C_{i0}	Initial substrate/metabolite conc (mg/dL, mM)
C_{iF}	Substrate/metabolite conc. into CBR (mg/dL, mM)
C_L	Lactate concentration (mM)
$C_{L,\max}$	Critical lactate concentration (mM)
D'	Dilution rate into chamber (h^{-1})
d_{cell}	Cell diameter
ε	Effective porosity
K_M	Monod constant (cm)
$K_{c\varepsilon}$	Chamber shape constant @ constant ε ($s^{0.5}$)
K_{cQ}	Chamber shape constant @ constant Q_R ($cm^{1.5}$)
m	Ammonium order of inhibition
n	Lactate order of inhibition
η	Culture medium viscosity (cP)
ω	Angular velocity (s^{-1})
ρ_{cell}	Cell density (g/cm^3)
ρ_{fluid}	Culture medium density (g/mL)
$\overline{\rho}_{susp}$	Suspension density (g/cm^3)
Q_F	Fresh feed flow rate (mL/min)
Q_R	Recycle flow rate (mL/min)
r_c	Conical chamber radius (cm)
r_{rotor}	Rotor disc radius (cm)
t	Time (h)
μ	Specific growth rate (h^{-1})
$\mu_{\max}$	Maximum specific growth rate (h^{-1})
V_C	Cell chamber volume (mL)
v_{cell}	Cell setting velocity (cm/s)
V_{CSTR}	Continuous stirred tank reactor volume (mL)
V_{PFR}	Plug flow reactor volume (mL)
X	Conversion of substrate
Y_i	Substrate or metabolite yield $\left(\frac{mg/dL \text{ or } mM}{cell/mL}\right)$

AUTHOR CONTRIBUTIONS

Kitana M. Kaiphanliam: Conceptualization; data curation; formal analysis; funding acquisition; investigation; methodology; visualization; writing – original draft; writing – review and editing. **Brenden Fraser-Hevlin:** Data curation; formal analysis; funding acquisition; investigation; methodology; visualization; writing – original draft; writing – review and editing. **Eric S. Barrow:** Conceptualization; methodology; resources; writing – original draft; writing – review and editing. **William C. Davis:** Conceptualization; data curation; funding acquisition; investigation; methodology; project administration; resources; supervision; validation; writing – review and editing. **Bernard J. Van Wie:** Conceptualization; funding acquisition; investigation; methodology; project administration; resources; supervision; writing – original draft; writing – review and editing.

ACKNOWLEDGMENTS

We acknowledge support from NSF EAGER #1645249 and companion REU supplements for Monika Cewe, Anna Crowley, Madeline Curtis, Sara Moore, Zakora Moore, and Chloe Nichol who assisted in data collection. We thank Wilson Boots, Scott Hanson, Gary Held, and Miles Pepper at the Voiland College of Engineering & Architecture Machine Shop for CBR prototyping. We acknowledge Vaniah Foat and Abbie Underhill at SBI for assisting us in beta-testing their on-line DO sensors. Additional support came from the WSU Commercialization Gap Fund, the Palouse Club Cougar Cage pitch competition, and the Washington Research Foundation. To build the early-concept CBR, an apheresis machine was loaned to WSU by Terumo BCT (formerly COBE Laboratories). We also thank the WSU College of Veterinary Medicine for taking care of the source of our CTL line, Steer #47157, who we imagine is now roaming happier fields.

CONFLICT OF INTEREST STATEMENT

The first author stands to benefit from the publication of this work, as it is a major part of her dissertation. Four of the authors are inventors on the non-provisional patent application submitted for the CBR technology and stand to benefit in the case the technology is commercialized. Two of the authors are co-founders of a startup that stands to benefit from the publication of this work in the case they secure licensing rights to the university-owned intellectual property.

PEER REVIEW

The peer review history for this article is available at https://www.webofscience.com/api/gateway/wos/peer-review/10.1002/btpr.3388.

DATA AVAILABILITY STATEMENT

The data that support the findings of this study are available from the corresponding author upon reasonable request.

ORCID

Kitana M. Kaiphanliam https://orcid.org/0000-0002-9799-0463
Brenden Fraser-Hevlin https://orcid.org/0000-0002-9982-4047
Eric S. Barrow https://orcid.org/0009-0006-2634-6319
William C. Davis https://orcid.org/0000-0002-3118-2228
Bernard J. Van Wie https://orcid.org/0000-0001-7382-9715

REFERENCES

1. Xu J, Murphy SL, Kochanek KD, Arias E. Mortality in the United States, 2021. 2022:8. NCHS Data Brief. https://www.cdc.gov/nchs/data/databriefs/db456.pdf
2. World Health Organization. The Top 10 Causes of Death. 2020. https://www.who.int/news-room/fact-sheets/detail/the-top-10-causes-of-death
3. Rosenblum D, Joshi N, Tao W, Karp JM, Peer D. Progress and challenges towards targeted delivery of cancer therapeutics. *Nature Communications*. 2018;9(1):1410. doi:10.1038/s41467-018-03705-y
4. Farhood B, Najafi M, Mortezaee K. CD8+ cytotoxic T lymphocytes in cancer immunotherapy: a review. *J Cell Physiol*. 2019;234(6):8509-8521. doi:10.1002/jcp.27782
5. Morotti M, Albukhari A, Alsaadi A, et al. Promises and challenges of adoptive T-cell therapies for solid tumours. *Br J Cancer*. 2021;124(11):1759-1776. doi:10.1038/s41416-021-01353-6
6. Wilson Wolf Manufacturing Corp. G-Rex: The Gold Standard for T Cell Therapy. Accessed June 15, 2022. https://www.wilsonwolf.com/g-rex-t-cell/
7. Cytiva Life Sciences. Xuri Cell Expansion System W25. Accessed June 15, 2022. https://www.cytivalifesciences.com/en/us/shop/cell-therapy/systems/xuri-cell-expansion-system-w25-p-06192
8. Miltenyi Biotec. Automated cell manufacturing on a closed and scalable platform. Accessed June 15, 2022. https://www.miltenyibiotec.com/US-en/products/cell-manufacturing-platform/clinimacs-prodigy-platform.html#gref
9. Lonza Group. Moving personalized medicine forward. Accessed June 15, 2022. https://pharma.lonza.com/technologies-products/cocoon-platform/cocoon
10. Bielser J-M, Wolf M, Souquet J, Broly H, Morbidelli M. Perfusion mammalian cell culture for recombinant protein manufacturing – a critical review. *Biotechnol Adv*. 2018;36(4):1328-1340. doi:10.1016/j.biotechadv.2018.04.011
11. Urdahl SG. COBE spectra apheresis system: designs, protocols and results. *Infusionstherapie*. 1989;16(Suppl 2):30-43.
12. Van Wie BJ, Brouns TM, Elliott ML, Davis WC. A novel continuous centrifugal bioreactor for high-density cultivation of mammalian and microbial cells. *Biotechnol Bioeng*. 1991;10:1190-1202.
13. Detzel CJ, Mason DJ, Davis WC, Van Wie BJ. Kinetic simulation of a centrifugal bioreactor for high population density hybridoma culture. *Biotechnol Prog*. 2009;25(6):1650-1659. doi:10.1002/btpr.240
14. Robergs RA, McNulty CR, Minett GM, Holland J, Trajano G. Lactate, not lactic acid, is produced by cellular cytosolic energy catabolism. *Physiology (Bethesda)*. 2018;33(1):10-12. doi:10.1152/physiol.00033.2017
15. Van Wie BJ, Elliott ML, Lee JM. Development and characterization of a continuous centrifugal bio-reactor. Presented at. *Biotechnol Bioeng Symp*. 1986;17: 335-344.
16. Van Wie BJ, Kaiphanliam KM, Fraser-Hevlin B, Barrow ES. inventors; Miniaturized Centrifugal Bioreactor and Rotor System (Application). Patent application 20220154125. 2022.
17. Van Wie BJ, Elliott ML, Brouns TM. inventors; Method and Apparatus for Continuous Centrifugal Bioprocessing. United States patent application US Patent 4939087. 1990.
18. Du X, Shi Y, Jegatheesan V, Haq IU. A review on the mechanism, impacts and control methods of membrane fouling in MBR system. *Membranes (Basel)*. 2020;10(2): 1-33. doi:10.3390/membranes10020024
19. Pinto NDS, Brower M. Wide-surface pore microfiltration membrane drastically improves sieving decay in TFF-based perfusion cell culture and streamline chromatography integration for continuous bioprocessing. *Biotechnol Bioeng*. 2020;117(11):3336-3344. doi:10.1002/bit.27504
20. US Food and Drug Administration. Yescarta: Highlights of Prescribing Information. 2017. 1.
21. Technologies S. Centrifugation Speed and Time for Cells. Accessed January 17, 2023.
22. Wu Y, Fan Z, Lu Y. Bulk and interior packing densities of random close packing of hard spheres. *J Mater Sci*. 2003;38(9):2019-2025. doi:10.1023/A:1023597707363
23. Detzel CJ, Van Wie BJ, Ivory CF. Fluid flow through a high cell density fluidized-bed during centrifugal bioreactor culture. *Biotechnol Prog*. 2010;26(4):1014-1023. doi:10.1002/btpr.395
24. McClelland RE, Dennis R, Reid LM, Stegemann JP, Palsson B, Macdonald JM. Chapter 6 – tissue engineering. In: Enderle JD, Bronzino JD, eds. *Introduction to Biomedical Engineering (Third Edition)*. Academic Press; 2012:273-357.
25. Carswell KS, Papoutsakis ET. Culture of human T cells in stirred bioreactors for cellular immunotherapy applications: shear, proliferation, and the IL-2 receptor. *Biotechnol Bioeng*. 2000;68(3):328-338. doi:10.1002/(SICI)1097-0290(20000505)68:33.0.CO;2-V
26. Costariol E, Rotondi M, Amini A, et al. Establishing the scalable manufacture of primary human T-cells in an automated stirred-tank bioreactor. *Biotechnol Bioeng*. 2019;116(10):2488-2502. doi:10.1002/bit.27088
27. Zhan C, Hagrot E, Brandt L, Chotteau V. Study of hydrodynamics in wave bioreactors by computational fluid dynamics reveals a resonance phenomenon. *Chem Eng Sci*. 2019;193:53-65. doi:10.1016/j.ces.2018.08.017
28. Detzel CJ, Thorson MR, Van Wie BJ, Ivory CF. A study of the Coriolis effect on the fluid flow profile in a centrifugal bioreactor. *Biotechnol Prog*. 2009;25(4):1025-1034. doi:10.1002/btpr.183
29. Maude AD, Whitmore RL. Theory of the flow of blood in narrow tubes. *J Appl Physiol*. 1958;12(1):105-113. doi:10.1152/jappl.1958.12.1.105
30. Fry LM, Schneider DA, Frevert CW, Nelson DD, Morrison WI, Knowles DP. East Coast fever caused by *Theileria parva* is characterized by macrophage activation associated with vasculitis and respiratory failure. *PloS One*. 2016;11(5):e0156004. doi:10.1371/journal.pone.0156004
31. Tretina K, Gotia HT, Mann DJ, Silva JC. Theileria-transformed bovine leukocytes have cancer hallmarks. *Trends Parasitol*. 2015;31(7):306-314. doi:10.1016/j.pt.2015.04.001
32. Elnaggar MM, Knowles DP, Davis WC, Fry LM. Flow cytometric analysis of the cytotoxic T-cell recall response to *Theileria parva* in cattle following vaccination by the infection and treatment method. *Vet Sci*. 2021;8(6):114. doi:10.3390/vetsci8060114
33. Doran PM. *Bioprocess Engineering Principles*. 2nd ed. Elsevier; 2013.
34. Han K, Levenspiel O. Extended monod kinetics for substrate, product, and cell inhibition. *Biotechnol Bioeng*. 1988;32(4):430-447. doi:10.1002/bit.260320404
35. Dimeloe S, Burgener AV, Grählert J, Hess C. T-cell metabolism governing activation, proliferation and differentiation; a modular view. *Immunology*. 2017;150(1):35-44. doi:10.1111/imm.12655
36. Ben Yahia B, Malphettes L, Heinzle E. Macroscopic modeling of mammalian cell growth and metabolism. *Appl Microbiol Biotechnol*. 2015;99(17):7009-7024. doi:10.1007/s00253-015-6743-6
37. Huynh HT, Robitaille G, Turner JD. Establishment of bovine mammary epithelial cells (MAC-T): an in vitro model for bovine lactation. *Exp Cell Res*. 1991;197(2):191-199. doi:10.1016/0014-4827(91)90422-Q
38. De Boer RJ, Homann D, Perelson AS. Different dynamics of $CD4_+$ and $CD8_+$ T cell responses during and after acute lymphocytic choriomeningitis virus infection. *J Immunol*. 2003;171(8):3928-3935. doi:10.4049/jimmunol.171.8.3928
39. Schlub TE, Sun JC, Walton SM, et al. Comparing the kinetics of NK cells, CD4, and CD8 T cells in murine cytomegalovirus infection. *J Immunol*. 2011;187(3):1385-1392. doi:10.4049/jimmunol.1100416
40. Xing Z, Bishop N, Leister K, Li ZJ. Modeling kinetics of a large-scale fed-batch CHO cell culture by Markov chain Monte Carlo method. *Biotechnol Prog*. 2010;26(1):208-219. doi:10.1002/btpr.284

41. Sigma M. Glucose in Cell Culture. Accessed January 17, 2022. https://www.sigmaaldrich.com/US/en/technical-documents/technical-article/cell-culture-and-cell-culture-analysis/mammalian-cell-culture/glucose
42. Furuichi Y, Kawabata Y, Aoki M, Mita Y, Fujii NL, Manabe Y. Excess glucose impedes the proliferation of skeletal muscle satellite cells under adherent culture conditions. *Front Cell Dev Biol*. 2021;9:640399. doi:10.3389/fcell.2021.640399
43. Barbieri L, Veliça P, Gameiro PA, et al. Lactate exposure shapes the metabolic and transcriptomic profile of CD8+ T cells. *Front Immunol*. 2023;14:1-16. doi:10.3389/fimmu.2023.1101433
44. Feng L, Liao H, Liu J, et al. Inhibition of PI3K/Akt/mTOR pathway by ammonium chloride induced apoptosis and autophagy in MAC-T cell. *Res Vet Sci*. 2021;136:622-630. doi:10.1016/j.rvsc.2021.01.020
45. Henry O, Kwok E, Piret JM. Simpler noninstrumented batch and semi-continuous cultures provide mammalian cell kinetic data comparable to continuous and perfusion cultures. *Biotechnol Prog*. 2008;24(4):921-931. doi:10.1002/btpr.17
46. Wen J, Cheng S, Zhang Y, et al. Lactate anions participate in T cell cytokine production and function. *Sci China Life Sci*. 2021;64(11):1895-1905. doi:10.1007/s11427-020-1887-7
47. Manstein F, Ullmann K, Kropp C, et al. High density bioprocessing of human pluripotent stem cells by metabolic control and in silico modeling. *Stem Cells Transl Med*. 2021;10(7):1063-1080. doi:10.1002/sctm.20-0453

How to cite this article: Kaiphanliam KM, Fraser-Hevlin B, Barrow ES, Davis WC, Van Wie BJ. Development of a centrifugal bioreactor for rapid expansion of CD8 cytotoxic T cells for use in cancer immunotherapy. *Biotechnol. Prog*. 2023; e3388. doi:10.1002/btpr.3388